

ties and interactive prompts. SAM 2 [34] extends promptable segmentation from the image to the video domain by introducing a memory mechanism to enhance temporal consistency, achieving remarkable performance in VOS. However, its application to RVOS presents several challenges.

First, the inherent absence of textual prompts in SAM 2’s architecture hinders the delivery of accurate prompts that align with the provided textual descriptions, as shown in Fig. 1 (a). Although some efforts have explored this area, further improvement is still needed. For instance, RefSAM [22] projects text embedding into sparse and dense prompts for SAM, but the sparse prompt from independent textual encoding fails to align with visual semantics, and the dense prompt lacks strong position cues like mask does. AL-RefSAM 2 [15] employs GPT-4 and Grounding DINO [24] to translate textual information into a box prompt of the target object, but the multi-stage pipeline heavily depends on the upstream model’s spatio-temporal reasoning ability, with substantial model parameters constraining deployment and inference efficiency of the model. Therefore, how to effectively align the vision-language features and provide accurate prompts to guide the decoding process is essential for adapting SAM 2 to RVOS. **Second**, the online-mode SAM 2 only has a historical view and cannot provide a global perspective for offline-mode RVOS, which may affect the global alignment of multimodal information and the temporal consistency of target objects. Consequently, effectively injecting global context information of the target objects into SAM 2 is crucial for RVOS.

To address these challenges, in this paper, we propose MPG-SAM 2, a novel end-to-end RVOS framework adapted from SAM 2. *The core idea is to align visual and textual features using an additional multimodal encoder, produce global context based on these multimodal features, and then inject them into SAM 2*, as shown in Fig. 1 (b). Concretely, we employ a unified multimodal encoder to jointly encode video and textual features, producing semantically aligned video and text embeddings, and multimodal class tokens. To provide accurate prompts for SAM 2, we devise a mask prior generator, which incorporates the video embeddings and multimodal class tokens to generate the pseudo masks of target objects for each frame in the video. These pseudo masks are then fed into the prompt encoder as the dense prompts, providing strong position priors to guide the mask decoding. Additionally, following [51], we sent the multimodal class tokens to the prompt encoder as the sparse prompts after MLP projection. By combining the powerful dense and sparse prompts, accurate prompts are provided to the mask decoder for better performance.

To introduce the global context of target objects into SAM 2, we design a hierarchical global-historical aggregator that allows SAM 2 to aggregate global context and historical information of target objects at multiple levels

before mask decoder. Here, the global context primarily comes from the global video feature generated by the mask prior generator. The aggregator consists of pixel and object-level fusion modules. In the pixel-level module, the current image feature interacts sequentially with the historical features in the memory of SAM 2 and the global context, thus enhancing the pixel-level target representation from various perspectives. Similarly, in the object-level module, the mask tokens aggregate target representation information from the global video feature and historical mask tokens in memory to generate the object tokens for the mask decoder.

Experimental results on several RVOS benchmarks demonstrate the state-of-the-art performance of our model and the effectiveness of our proposed modules. The main contributions of this work can be summarized as follows:

- We propose a novel RVOS framework, MPG-SAM 2, adapted from SAM 2 by introducing mask prior-based dense prompt and multi-level global context fusions, achieving cutting-edge performance on several RVOS benchmarks.
- We devise a mask prior generator that leverages the global video feature and multimodal class tokens to produce pseudo masks of target objects, providing the prior position cues as dense prompts for SAM 2 to enhance the mask decoding.
- We develop a hierarchical global-historical aggregator that integrates global context and historical memory information of target objects into SAM 2 at both pixel and object levels. This module enables the online SAM 2 to have a global view and enhances the target representation and temporal consistency.

2. Related work

Referring Video Object Segmentation. RVOS attracts extensive interest as it bridges visual and linguistic domains. Early methods, such as RefVOS [2], consider RVOS as an expansion of referring image segmentation (RIS) to the video domain. URVOS [35] advances this by combining RIS and semi-supervised video object segmentation within a unified framework using attention mechanisms. In subsequent studies [12, 21, 28, 38, 40], researchers emphasize cross-modal interaction, further enhancing RVOS performance. However, despite notable gains, the computational expense and complexity of multi-stage pipelines limit practical feasibility. In response, query-based Transformer architectures offer efficient solutions with simplified yet robust frameworks. Notably, MTTR [3] and ReferFormer [42] pioneer the use of the DETR series [5, 52] in RVOS, introducing novel multimodal interaction mechanisms. Recent methods [20, 26, 29, 36] refine these Transformer architectures through advanced temporal and multimodal feature integration techniques. For instance, SgMg [29] enhances ReferFormer by replacing dynamic convolution with a seg-

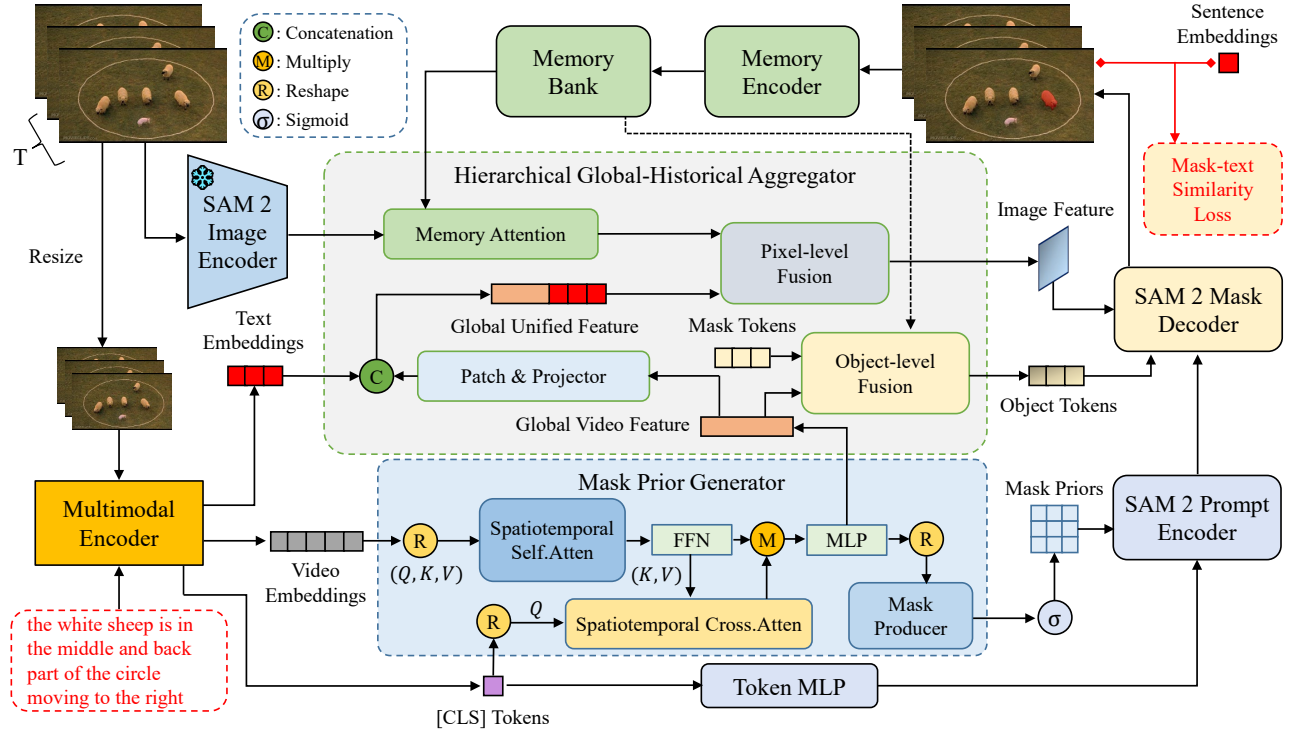


Figure 2. The overview of the proposed MPG-SAM 2. It mainly consists of four parts: the multimodal encoder, the mask prior generator, the hierarchical global-historical aggregator, and the SAM 2. After projection, the jointly encoded multimodal [CLS] tokens serve as the sparse prompts for SAM 2. The mask prior generator generates pseudo masks of target objects as the dense prompts and produces the global video feature as the global context. The global-historical aggregator aggregates the target information from the global context and memory features to enhance the target representation of pixel-level image features and object-level object tokens. The mask-text similarity loss constrains the correlation between object masks and textual features.

mentation optimizer and uses spectral information to guide visual feature fusion. SOC [26] implements layered temporal modeling across video and object levels, achieving early multimodal fusion. More recently, Losh [48] introduces a joint prediction network for short and long sentences, reducing the over-influence of action and relational cues in segmentation. To tackle longer sequences and complex scenarios in the MeViS [11] dataset, DsHmp [14] proposes a static text decoupling strategy, enhancing the temporal understanding of static and dynamic content at both frame and object levels, thereby capturing both short-term and long-term motion insights.

Segment Anything Model. SAM [18] is an interactive segmentation model capable of generating non-semantic masks based on various prompts. Trained on a large-scale dataset, SAM exhibits strong generalization across a wide range of common objects. Several variants [16, 43, 50] have focused on improving the segmentation accuracy and computational efficiency of SAM. Moreover, SAM has found widespread application in various fields, including video tracking [8], remote sensing image interpretation [37], and medical image processing [49]. Recently, SAM 2 [16] ex-

tends SAM to the video domain, achieving state-of-the-art performance. Despite its excellence in visual segmentation tasks using box, point, or mask prompts, SAM lacks language comprehension capabilities and cannot directly handle referring segmentation tasks. With the advancement of multimodal large language models (MLLMs), recent approaches [19, 33, 44] utilize MLLMs to encode textual guidance for SAM segmentation. Specifically, LISA [19] fine-tunes LLaVA [23] to generate multimodal features by extracting hidden embeddings based on specific prompts. u-LLaVA [44] extends this approach to enable joint multi-task processing at region and pixel levels. GLaMM [33] integrates the visual grounding task and incorporates language responses to provide multi-granular segmentation prompts to the model. Most recently, EVF-SAM [51] introduces a lightweight pre-fusion architecture that employs joint visual-language encoding to generate high-quality textual prompts, leading to excellent segmentation performance.

3. Method

3.1. Overview

The overview of our proposed MPG-SAM 2 is illustrated in Fig. 2. MPG-SAM 2 consists of four primary components: the multimodal encoder, the mask prior generator, the hierarchical global-historical aggregator, and the SAM 2. Given a video sequence $\mathcal{V} = \{I_t\}_{t=1}^T$ with T frames and its corresponding textual description $\mathcal{E} = \{e_l\}_{l=1}^L$ with L words, the multimodal encoder first performs joint encoding independently across frames, extracting the multimodal [CLS] tokens, the video patch embeddings and the text embeddings. Simultaneously, the image encoder of SAM 2 independently extracts video features. The mask prior generator receives the video patch embeddings and multimodal [CLS] tokens, generates the global video feature, and produces prior masks for each frame. These prior masks along with the multimodal [CLS] tokens, serve as the prompts for SAM 2. The hierarchical global-historical aggregator integrates the global video feature, text embeddings, and the historical mask features and tokens from SAM 2’s memory to hierarchically enhance the target representations of pixel-level image features and object-level object tokens. Finally, SAM 2’s decoder performs online decoding based on the provided prompts, object tokens, and current image features to obtain precise object masks for the current frame.

3.2. Feature Extraction

Aligning the visual-linguistic space is critical for the RVOS task. Following EVF-SAM [51] and Shared-RIS [47], we employ a unified visual-linguistic encoder, BEiT-3 [39], to jointly encode video and language features. Each input video frame for multimodal encoder $I_m \in \mathbb{R}^{H_m \times W_m \times 3}$ is reshaped into a sequence of flattened image patches $V_p \in \mathbb{R}^{N_v \times (p^2 \times 3)}$ and transformed through a projection layer to $V_p \in \mathbb{R}^{N_v \times D}$. Here, H_m, W_m represent the height and width of the multimodal encoder’s input size, respectively. $N_v = \frac{H_m \times W_m}{p^2}$ denotes the number of patches, where p is the patch size and D is the channel size of the multimodal encoder. A visual class token $V_{cls} \in \mathbb{R}^{1 \times D}$ is then prepended, followed by the addition of learnable visual positional embeddings $V_{pos} \in \mathbb{R}^{(N_v+1) \times D}$, resulting in the visual patch embeddings $V_0 \in \mathbb{R}^{(N_v+1) \times D}$. Concurrently, the text input of length L is tokenized using XLMRoberta-Tokenizer [9], generating tokenized result T_{tok} , with a class token $T_{cls} \in \mathbb{R}^{1 \times D}$ and an end-of-token marker $T_{end} \in \mathbb{R}^{1 \times D}$ appended to the start and end, respectively. Following this, learnable positional embeddings $T_{pos} \in \mathbb{R}^{N_l \times D}$ similar to the visual patch embeddings are added to obtain the text embeddings $T_0 \in \mathbb{R}^{N_l \times D}$, where $N_l = L + 2$ denotes the length of text embeddings. By concatenating the visual patch embeddings V_0 with the text embeddings T_0 , we obtain the joint visual-text embedding G_0 . The entire

process can be represented by the following equation:

$$\begin{aligned} V_0 &= [V_{cls}, V_p] + V_{pos}, \\ T_0 &= [T_{cls}, T_{tok}, T_{end}] + T_{pos}, \\ G_0 &= [V_0; T_0] \in \mathbb{R}^{(N_v+N_l+1) \times D}. \end{aligned} \quad (1)$$

Following multimodal fusion through multiple attention blocks, the joint visual-text embedding is fed into modality-specific feedforward neural networks (FFNs) for vision and text. We ultimately obtain the joint visual-text embeddings $G \in \mathbb{R}^{T \times (N_v+N_l+1) \times D}$ for the entire video, which are then decomposed into the multimodal [CLS] tokens $V_{cls} \in \mathbb{R}^{T \times 1 \times D}$, video patch embeddings $V \in \mathbb{R}^{T \times N_v \times D}$, and text embeddings $T \in \mathbb{R}^{T \times N_l \times D}$.

Meanwhile, The SAM 2 image encoder performs frame-independent encoding on each input video frame $I_s \in \mathbb{R}^{H_s \times W_s \times 3}$. For the i -th frame, a set of hierarchical multi-scale features is extracted for mask generation, with the final layer image feature $F_i \in \mathbb{R}^{\frac{H_s}{16} \times \frac{W_s}{16} \times C}$ serving as the input for the subsequent decoding process, where H_s, W_s and C denote the height and width of the input image, and the channel of SAM 2 image encoder, respectively.

3.3. Mask Prior Generator

While the semantic alignment between video patch embeddings V and text embeddings T proves effective, the SAM video features F lack inherent linguistic context, creating a semantic disparity with the text features. Furthermore, the frame-agnostic nature of [CLS] tokens encoding limits their capacity to capture video-level temporal dynamics, potentially causing segmentation inaccuracies such as object misalignment and displacement. To mitigate these limitations, we propose generating frame-specific pseudo mask priors by integrating the [CLS] tokens with language-enhanced video patch embeddings. These priors, providing pixel-level guidance, refine the SAM 2 decoding process.

As illustrated in Fig. 2, we start by establishing inter-frame interaction among the video patch embeddings for each frame. Frame-agnostic video patch embeddings are temporally and spatially unfolded into video embeddings $V' \in \mathbb{R}^{(T \times N_v) \times D}$, which are subsequently fed into the multi-head self-attention layer and feed-forward network (FFN) to model the spatiotemporal context across the $T \times N_v$ dimension, learning pixel-wise inter-frame global correlations. Afterward, the [CLS] tokens for each frame are similarly flattened across the spatiotemporal dimensions, resulting in video class embeddings $V'_{cls} \in \mathbb{R}^{(T \times 1) \times D}$. To generate frame-consistent mask priors while enriching the class embeddings with visual context, we employ a multi-head cross-attention to facilitate spatiotemporal interaction between the video class embedding and the video patch embeddings. Here, the video class embeddings V'_{cls} serve as queries, while the video embeddings V' act as keys and val-

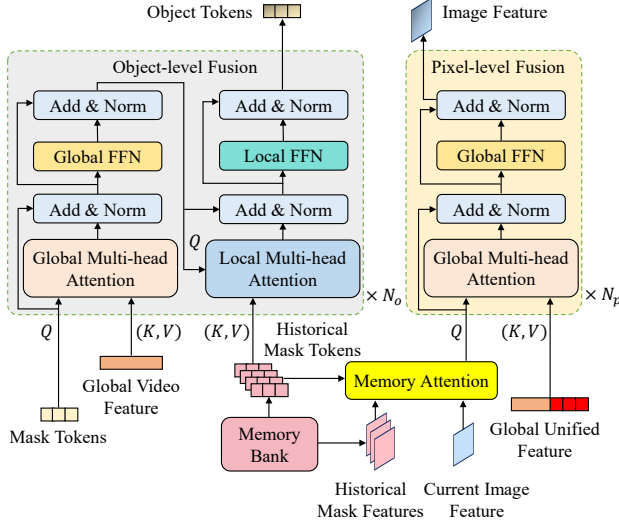


Figure 3. The structure of the hierarchical global-historical aggregator.

ues. Formulation of the whole process proceeds as follows:

$$\begin{aligned} V' &= R(V) + \text{softmax} \left(R(V)R(V)^T / \sqrt{D} \right) \cdot R(V), \\ V'_{cls} &= R(V_{cls}) + \text{softmax} \left(R(V_{cls})V'^T / \sqrt{D} \right) \cdot V', \end{aligned} \quad (2)$$

where $R(\cdot)$ denotes the reshape operation and D represents the channel dimension of embeddings.

The preceding steps establish inter-frame coherence in both video patch embeddings V and class embeddings V_{cls} . The class embeddings V_{cls} , jointly encoded with visual and linguistic modalities, effectively represent the intersection of visual and textual information, specifically the object denoted in the text. Therefore, after the video class embeddings V'_{cls} are broadcast to match the dimensions of the video embeddings V' , element-wise multiplication is performed. The resulting embeddings are then processed by a MLP layer to generate the global video feature V_g enriched with object information. Simultaneously, dimensionality reduction is applied to both the video and class embeddings. The video embeddings are reshaped into feature maps with dimensions $\frac{H_m}{p} \times \frac{W_m}{p}$. The class embeddings V_{cls} , representing foreground information, are multiplied element-wise with these reshaped video embeddings representing global features. This product is subsequently passed through the mask producer, which consists of a MLP layer and a sigmoid activation function, to generate the frame-specific mask priors $M_p \in \mathbb{R}^{T \times \frac{H_m}{p} \times \frac{W_m}{p}}$. The formal description of this process is provided below:

$$V_g = \text{MLP}(V' \cdot V'_{cls}), M_p = \sigma(\text{MLP}(V_g)), \quad (3)$$

where σ represents the sigmoid function.

The global video feature V_g , enriched with object information, are input to the hierarchical global-historical aggregator, thereby integrating global object context. Frame-specific mask priors M_p are upsampled to the dimensions H_s and W_s , matching the feature map size of the SAM 2 decoder, via linear interpolation. These upsampled priors are then supplied as dense prompts to the SAM 2 prompt encoder.

3.4. Hierarchical Global-Historical Aggregator

Unlike VOS, which focuses on frame-specific features, RVOS emphasizes foreground information and the effective use of temporal and textual cues. Inspired by [7], we design a hierarchical global-historical aggregator with SAM 2's memory mechanism, which integrates global frame features and past segmentation results while embedding temporal information into both pixel and object levels. This approach enables better communication between high-level and low-level representations, improving the overall segmentation accuracy.

Fig. 3 illustrates the structure of the hierarchical global-historical aggregator. In the pixel-level fusion part, the global-historical aggregator is integrated with the memory mechanism from SAM 2. The memory bank, containing mask features F_{mh} and mask tokens T_{mh} from historical frames, brings localized temporal information from past frames to the video features.

For global information enhancement, SAM 2 video features F lack guidance from textual information, which poses a challenge for facilitating effective information exchange from the object level to the pixel level. To address this, the global video feature V_g is further partitioned into patches of size p_g and compressed via MLP layers to remove redundancy. These compressed patches are concatenated with each frame's corresponding text features, resulting in the global unified feature V_u . Although each frame's text features are independently encoded, their semantics correspond to the entire video and can thus be considered part of the global information.

For the current image feature F_i of the i -th frame, memory attention is first performed with the historical mask features F_{mh} and historical mask tokens T_{mh} in the memory bank. This is followed by cross-attention with the global unified features V_u . After an add operation, a layer norm, and a global FFN layer, this process yields the current frame feature F_{gl} with alternating global and local enhancements. The entire process is illustrated as follows:

$$\begin{aligned} F'_i &= \text{Mematten}(F_i, F_{mh}, T_{mh}) \\ F_{gl} &= F'_i + \text{softmax} \left(F'_i V_u^T / \sqrt{C} \right) \cdot V_u, \end{aligned} \quad (4)$$

where $\text{Mematten}(\cdot)$ represents the SAM 2 memory attention, and C denotes the channel dimension of the SAM 2

feature.

For the object-level fusion, the current frame mask tokens T_m first undergo cross-attention with the global video feature V_g from the mask prior generator, followed by an add operation, a layer norm, and a global FFN layer. Subsequently, the globally enhanced mask token T_{mg} performs cross-attention with historical mask tokens T_{mh} , which are stored in the memory bank with enriched mask information. This is followed by an add operation, a layer norm, and a local FFN layer, producing the object token T_{mgl} with both global and historical enhancements. The overall process is depicted as follows:

$$\begin{aligned} T_{mg} &= T_m + \text{softmax}\left(T_m V_g^T / \sqrt{C}\right) \cdot V_g, \\ T_{mgl} &= T_{mg} + \text{softmax}\left(T_{mg} T_{mh}^T / \sqrt{C}\right) \cdot T_{mh}, \end{aligned} \quad (5)$$

here, C denotes the channel dimension of mask tokens.

The enhanced object tokens T_{mgl} are then fed into the mask decoder, replacing the original mask tokens within the decoder, while the augmented current image feature F_{gl} is also passed into the mask decoder for decoding. In this manner, both the object queries and video features are enriched with temporal information, facilitating a comprehensive understanding of the entire video from both high-level and low-level perspectives. This ensures effective communication between pixel-level and object-level representations.

3.5. SAM 2 Prompt Encoder and Mask Decoder

In MPG-SAM 2, the SAM 2 prompt encoder accepts two types of prompts: dense prompts M_p generated by the mask prior generator and sparse prompts V_{cls} from the multimodal encoder. Inspired by EVF-SAM [51], we follow a similar approach to SAM 2’s handling of point and box prompts by projecting the [CLS] tokens V_{cls} through token MLP and then concatenating them with zero-initialized sparse embeddings. For pixel-level prompts M_p , after ensuring that their spatial dimensions match those of the SAM 2 feature, they are fed as dense spatial prompts into the mask decoder.

The SAM 2 mask decoder receives both sparse object-level prompts and dense pixel-level prompts. The sparse prompts are concatenated with the object tokens to act as the object-level query for the decoder, while the dense pixel-level prompts, which serve as the generated mask prompts, are added element-wise to the video frame features, guiding decoding directly from high-resolution feature layers.

Although SAM 2 does not natively support simultaneous input of both sparse and dense prompts, combining multimodal sparse embeddings with pixel-level pseudo mask priors enhances the mask decoder’s ability to interpret objects referenced in text, which is essential for RVOS tasks. Con-

sequently, we have modified SAM 2 to support both prompt types concurrently.

3.6. Training Loss

MPG-SAM 2 employs an overall loss function similar to that of [42] to constrain the predicted mask as follows:

$$\mathcal{L} = \lambda_{dice} \mathcal{L}_{dice} + \lambda_{focal} \mathcal{L}_{focal} + \lambda_{sim} \mathcal{L}_{sim}, \quad (6)$$

here, \mathcal{L}_{dice} is the DICE loss [30], \mathcal{L}_{focal} represents the binary mask focal loss and \mathcal{L}_{sim} denotes the mask-text similarity loss, which is a loss function designed to constrain the similarity between the mask and the text. For detailed information, please refer to the appendix.

4. Experiments

4.1. Datasets and Metrics

Datasets. The experiments are performed on several key RVOS datasets: Ref-YouTube-VOS [35], MeViS [11] and Ref-DAVIS17 [17]. Ref-YouTube-VOS is a widely recognized and large-scale dataset in the field of RVOS, containing 3471 videos with 12913 expressions in the training set and 202 videos with 2096 expressions in the validation set. MeViS, a newly established dataset, focuses on motion analysis, consisting of 2,006 videos with 28,570 annotations. Ref-DAVIS17 builds on the DAVIS17 [32] dataset with additional linguistic annotations for diverse objects, comprising 90 videos.

Evaluation Metrics. We adhere to the standard evaluation framework outlined in [35], employing metrics such as region similarity J , contour accuracy F , and their combined average $J\&F$ to evaluate our model on the validation sets of Ref-Youtube-VOS, MeViS and Ref-DAVIS17. Due to the absence of publicly accessible ground truth annotations for the Ref-Youtube-VOS and MeViS validation set, we utilize the official server to submit our predictions and obtain the evaluation results.

4.2. Implementation Details

Model Settings. We initialize the relevant modules of SAM 2 and the multimodal encoder using the SAM 2-Hiera-Large [34] and BEiT-3-Large [39] pre-trained weights. For feature parsing, each image is resized to resolutions of 1024×1024 and 224×224 , serving as the input to SAM 2 image encoder with an output dimension C of 256, and the multimodal encoder with an output dimension D of 1024, respectively. In the hierarchical global-historical aggregator, the patch size p_g for the global video feature in pixel-level fusion is set to 2. Both the pixel-level fusion layer number N_p and object-level fusion layer number N_o are set to 1. The memory bank is configured similarly to SAM 2 [34], with a maximum storage capacity of 7 historical mask features and 16 mask tokens.

Table 1. Comparison with state-of-the-art methods on the Ref-YouTube-VOS and Ref-DAVIS17 datasets.

Method	Reference	Ref-YouTube-VOS			Ref-DAVIS17		
		$\mathcal{J}\&\mathcal{F}$	\mathcal{J}	\mathcal{F}	$\mathcal{J}\&\mathcal{F}$	\mathcal{J}	\mathcal{F}
ReferFormer [42]	CVPR'22	62.9	61.3	64.6	61.1	58.1	64.1
OnlineRefer [41]	ICCV'23	62.9	61.0	64.7	62.4	59.1	65.6
HTML [13]	ICCV'23	63.4	61.5	65.2	62.1	59.2	65.1
SgMg [29]	ICCV'23	65.7	63.9	67.4	63.3	60.6	66.0
TempCD [36]	ICCV'23	65.8	63.6	68.0	64.6	61.6	67.6
SOC [26]	NIPS'23	66.0	64.1	67.9	64.2	61.0	67.4
DsHmp [14]	CVPR'24	67.1	65.0	69.1	64.9	61.7	68.1
LoSh [48]	CVPR'24	67.2	65.4	69.0	64.3	61.8	66.8
MUTR [45]	AAAI'24	68.4	66.4	70.4	68.0	64.8	71.3
MPG-SAM 2	-	73.9	71.7	76.1	72.4	68.8	76.0

Training Details. Experiments are conducted on 8 NVIDIA A800 GPUs for the MeViS [11] dataset due to its high memory requirements stemming from dataset-specific configuration and on 8 NVIDIA GeForce RTX 4090 GPUs for the remaining datasets. The MeViS dataset experiments follow settings similar to [14], with 8 frames as input for training, and are trained directly on this dataset without any pre-training on RefCOCO+/g [27, 46]. Training is performed for 6 epochs using the AdamW optimizer [25], set at a learning rate of $2e-6$. For the Ref-YouTube-VOS [35] and Ref-DAVIS17 [17] datasets, we adopt an approach similar to [29, 42], first pre-training on the RefCOCO+/g [27, 46] for 10 epochs, followed by fine-tuning on Ref-YouTube-VOS for 6 epochs. The batch size during pre-training is set to 8, with a learning rate of $1e-5$, while fine-tuning use a batch size of 1, a learning rate of $2e-6$, and 5 frames as input. To better align with the pre-trained parameters of other modules, we set a learning rate of $5e-5$ for both the hierarchical global-historical aggregator and the mask prior generator. The trained model is then validated on the Ref-DAVIS17 dataset without additional training. The loss weights for different losses are set as follows: $\lambda_{focal} = 2$, $\lambda_{dice} = 5$, and $\lambda_{sim} = 2$.

4.3. Comparison with State-of-the-Art Methods

Ref-YouTube-VOS & Ref-DAVIS17 sets. We conduct a comprehensive comparison between our method, MPG-SAM 2, and several state-of-the-art approaches. The results of the comparison are reported in Tab. 1. It can be observed that our approach, outperforms all existing approaches across these two benchmark datasets. On the Ref-YouTube-VOS dataset, it achieves 73.9% $\mathcal{J}\&\mathcal{F}$, surpassing the current best methods, DsHmp [14] by 6.8% and LoSh [48] by 6.7%. For approaches leveraging additional training data, our model also demonstrates competitive performance, exceeding MUTR [45] by 5.5% in $\mathcal{J}\&\mathcal{F}$. On the Ref-DAVIS dataset, our approach achieves a $\mathcal{J}\&\mathcal{F}$ score

Table 2. Comparison with state-of-the-art methods on the MeViS dataset.

Method	Reference	$\mathcal{J}\&\mathcal{F}$	\mathcal{J}	\mathcal{F}
URVOS [35]	ECCV'20	27.8	25.7	29.9
LBDT [12]	CVPR'22	29.3	27.8	30.8
MTTR [4]	CVPR'22	30.0	28.8	31.2
ReferFormer [42]	CVPR'22	31.0	29.8	32.2
VLT+TC [10]	TPAMI'22	35.5	33.6	37.3
LMPM [11]	ICCV'23	37.2	34.2	40.2
DsHmp [14]	CVPR'24	46.4	43.0	39.8
MPG-SAM 2	-	53.7	50.7	56.7

Table 3. Ablation study of different components of MPG-SAM 2 on Ref-YouTube-VOS dataset.

Method	MPG	HGA	$\mathcal{J}\&\mathcal{F}$	\mathcal{J}	\mathcal{F}
Baseline			70.3	68.3	72.2
MPG-SAM 2	✓		71.9	69.8	73.9
MPG-SAM 2		✓	72.3	70.1	74.4
MPG-SAM 2	✓	✓	73.9	71.7	76.1

of 72.4%, outperforming the leading method DsHmp by 7.5% and the top-performing additional data-trained model MUTR by 4.4%.

MeViS set. We also conduct comparative experiments between our MPG-SAM 2 and existing methods including URVOS [35], LBDT [12], MTTR [4], ReferFormer [42], VLT+TC [10], LMPM [11] and DsHmp [14], on the MeViS [11] dataset, with results documented in Tab. 2. On this dataset, our method achieves a $\mathcal{J}\&\mathcal{F}$ score of 53.7%, surpassing the current state-of-the-art method DsHmp by 7.3% $\mathcal{J}\&\mathcal{F}$, demonstrating the effectiveness of our approach in leveraging temporal information.

Fig. 4 presents the visual comparison of our MPG-SAM 2 model with SgMg [29] on Ref-YouTube-VOS dataset. The results clearly demonstrate that MPG-SAM 2 consistently surpasses SgMg, especially in prediction accuracy and maintaining frame-to-frame consistency.

4.4. Model Analysis

In this section, we conduct comprehensive ablation experiments to examine the effects of the key components of our MPG-SAM 2 and the influence of various model configurations. All experiments are carried out using the Ref-YouTube-VOS dataset.

Components Analysis. To explore the influence of the key components of our model, we first construct a baseline model consisting solely of SAM 2 and the multimodal encoder. As depicted in Tab. 3, when we add the mask prior

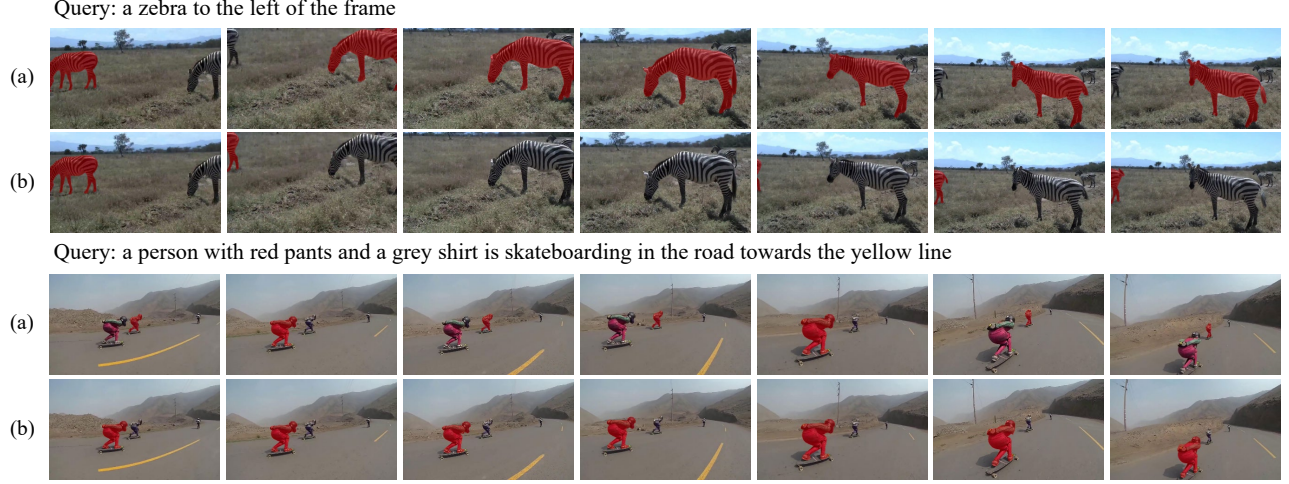


Figure 4. Visualization result on Ref-YouTube-VOS. (a) SgMg [29], (b) MPG-SAM 2. MPG-SAM 2 effectively ensures the global spatiotemporal consistency of masks, reducing objects misalignment and drift.

Table 4. Model analysis of different settings in MPG-SAM 2.

Method	Settings	$\mathcal{J}\&\mathcal{F}$	\mathcal{J}	\mathcal{F}
Interaction Mode of MPG				
MPG-SAM 2	w/o S_{si}	73.3	71.2	75.4
MPG-SAM 2	w/o S_{ci}	73.5	71.4	75.6
MPG-SAM 2	w $S_{si}\&S_{ci}$	73.9	71.7	76.1
Patch Size of HGA				
MPG-SAM 2	1	73.2	71.0	75.4
MPG-SAM 2	2	73.9	71.7	76.1
MPG-SAM 2	4	73.6	71.4	75.7
Global Video Feature of HGA				
MPG-SAM 2	Vanilla	73.1	71.1	75.1
MPG-SAM 2	Masked	73.9	71.7	76.1

generator (MPG) to the baseline model, the special MPG-SAM 2 achieves 71.9% $\mathcal{J}\&\mathcal{F}$, which is 1.6 higher than the baseline. While only the hierarchical global-historical aggregator (HGA) is imposed on the baseline, the $\mathcal{J}\&\mathcal{F}$ score of the special MPG-SAM 2 reaches 72.3%, indicating a 2.0 improvement and further validating the module’s superiority. With both components integrated, our MPG-SAM 2 delivers the best performance of 73.9% $\mathcal{J}\&\mathcal{F}$. Note that the memory mechanism is excluded from HGA during performance calculations; when the MPG module is omitted, only the mask prior is not generated, while the global video feature production remains.

Mask Prior Generator. In this section, we investigate different spatiotemporal interaction forms within the mask prior generator (MPG), with results presented in Tab. 4.

When the overall spatiotemporal self-interaction (S_{si}) of video embeddings is omitted, MPG-SAM 2 experiences a performance drop of 0.6% $\mathcal{J}\&\mathcal{F}$. Similarly, when the spatiotemporal cross-modal interaction (S_{ci}) between the [CLS] tokens and video embeddings is excluded, the model performance decreases by 0.4% $\mathcal{J}\&\mathcal{F}$. These findings highlight the importance of understanding video information from a global spatiotemporal perspective during the mask prompt generation process.

Hierarchical Global-Historical Aggregator. The impact of different settings of hierarchical global-historical aggregator (HGA) is also worth noting. First, we examine the effect of patch size p_g in the pixel-level fusion process for the global video feature, experimenting with patch sizes 1, 2, and 4. As shown in Tab. 4, the patch size of 2 yields the best model performance. This configuration achieves an optimal balance between critical and redundant information during pixel-level fusion, allowing for more effective integration of global context.

Additionally, we explore different configurations for the global video feature input to the hierarchical global-historical aggregator. One straightforward approach named “Vanilla” employs the video embeddings directly output by the multimodal encoder as the global feature. An alternative approach dubbed “Masked” leverages a video feature enriched with mask prior information. Results in Tab. 4 indicate that video features containing mask information are more beneficial for global context integration, as they better emphasize global frame mask information to guide the segmentation of the current frame.

5. Conclusion

In this paper, we present MPG-SAM 2, an innovative end-to-end framework for RVOS, to address the challenges of adapting SAM 2 to the RVOS task. Our approach utilizes a unified multimodal encoder to jointly encode video and textual features, generating semantically aligned video and text embeddings, along with multimodal class tokens. The video embeddings and class tokens are employed by a mask prior generator to create pseudo masks of target objects, offering strong positional cues as dense prompts for SAM 2’s mask decoder. To address SAM 2’s lack of global context awareness in offline RVOS, we introduce a hierarchical global-historical aggregator. This enables SAM 2 to integrate global context and historical information of target objects at both pixel and object levels, enhancing the target representation and temporal consistency. Extensive experiments on several RVOS benchmarks demonstrate the superiority of our MPG-SAM 2 over state-of-the-art methods and validate the effectiveness of our proposed modules.

References

- [1] Maksym Bekuzarov, Ariana Bermudez, Joon-Young Lee, and Hao Li. Xmem++: Production-level video segmentation from few annotated frames. In *Proceedings of the IEEE/CVF International Conference on Computer Vision*, pages 635–644, 2023. 1
- [2] Miriam Bellver, Carles Ventura, Carina Silberer, Ioannis Kazakos, Jordi Torres, and Xavier Giro-i Nieto. Refvos: A closer look at referring expressions for video object segmentation. *arXiv preprint arXiv:2010.00263*, 2020. 2
- [3] Adam Botach, Evgenii Zheltonozhskii, and Chaim Baskin. End-to-end referring video object segmentation with multimodal transformers. In *Proceedings of the IEEE Conference on Computer Vision and Pattern Recognition (CVPR)*, pages 4985–4995, 2022. 2
- [4] Adam Botach, Evgenii Zheltonozhskii, and Chaim Baskin. End-to-end referring video object segmentation with multimodal transformers. In *Proceedings of the IEEE/CVF Conference on Computer Vision and Pattern Recognition*, pages 4985–4995, 2022. 7
- [5] Nicolas Carion, Francisco Massa, Gabriel Synnaeve, Nicolas Usunier, Alexander Kirillov, and Sergey Zagoruyko. End-to-end object detection with transformers. In *Proceedings of the European Conference on Computer Vision (ECCV)*, pages 213–229, 2020. 2
- [6] Ho Kei Cheng and Alexander G Schwing. Xmem: Long-term video object segmentation with an atkinson-shiffrin memory model. In *European Conference on Computer Vision*, pages 640–658. Springer, 2022. 1
- [7] Ho Kei Cheng, Seoung Wug Oh, Brian Price, Joon-Young Lee, and Alexander Schwing. Putting the object back into video object segmentation. In *Proceedings of the IEEE/CVF Conference on Computer Vision and Pattern Recognition*, pages 3151–3161, 2024. 5
- [8] Yangming Cheng, Liulei Li, Yuanyou Xu, Xiaodi Li, Zongxin Yang, Wenguan Wang, and Yi Yang. Segment and track anything. *arXiv preprint arXiv:2305.06558*, 2023. 3
- [9] A Conneau. Unsupervised cross-lingual representation learning at scale. *arXiv preprint arXiv:1911.02116*, 2019. 4
- [10] Henghui Ding, Chang Liu, Suchen Wang, and Xudong Jiang. Vision-language transformer and query generation for referring segmentation. In *Proceedings of the IEEE/CVF International Conference on Computer Vision*, pages 16321–16330, 2021. 7
- [11] Henghui Ding, Chang Liu, Shuting He, Xudong Jiang, and Chen Change Loy. Mevis: A large-scale benchmark for video segmentation with motion expressions. In *Proceedings of the IEEE/CVF International Conference on Computer Vision*, pages 2694–2703, 2023. 3, 6, 7
- [12] Zihan Ding, Tianrui Hui, Junshi Huang, Xiaoming Wei, Jizhong Han, and Si Liu. Language-bridged spatial-temporal interaction for referring video object segmentation. In *Proceedings of the IEEE/CVF Conference on Computer Vision and Pattern Recognition*, pages 4964–4973, 2022. 2, 7
- [13] Mingfei Han, Yali Wang, Zhihui Li, Lina Yao, Xiaojun Chang, and Yu Qiao. Htm: Hybrid temporal-scale multimodal learning framework for referring video object segmentation. In *Proceedings of the IEEE/CVF International Conference on Computer Vision*, pages 13414–13423, 2023. 7
- [14] Shuting He and Henghui Ding. Decoupling static and hierarchical motion perception for referring video segmentation. In *Proceedings of the IEEE/CVF Conference on Computer Vision and Pattern Recognition*, pages 13332–13341, 2024. 3, 7
- [15] Shaofei Huang, Rui Ling, Hongyu Li, Tianrui Hui, Zongheng Tang, Xiaoming Wei, Jizhong Han, and Si Liu. Unleashing the temporal-spatial reasoning capacity of gpt for training-free audio and language referenced video object segmentation. *arXiv preprint arXiv:2408.15876*, 2024. 2
- [16] Lei Ke, Mingqiao Ye, Martin Danelljan, Yu-Wing Tai, Chi-Keung Tang, Fisher Yu, et al. Segment anything in high quality. *Advances in Neural Information Processing Systems*, 36, 2024. 1, 3
- [17] Anna Khoreva, Anna Rohrbach, and Bernt Schiele. Video object segmentation with language referring expressions. In *Proceedings of the Asian Conference on Computer Vision (ACCV)*, pages 123–141, 2018. 6, 7
- [18] Alexander Kirillov, Eric Mintun, Nikhila Ravi, Hanzi Mao, Chloe Rolland, Laura Gustafson, Tete Xiao, Spencer Whitehead, Alexander C Berg, Wan-Yen Lo, et al. Segment anything. In *Proceedings of the IEEE/CVF International Conference on Computer Vision*, pages 4015–4026, 2023. 1, 3
- [19] Xin Lai, Zhuotao Tian, Yukang Chen, Yanwei Li, Yuhui Yuan, Shu Liu, and Jiaya Jia. Lisa: Reasoning segmentation via large language model. In *Proceedings of the IEEE/CVF Conference on Computer Vision and Pattern Recognition*, pages 9579–9589, 2024. 3
- [20] Meng Lan, Fu Rong, Zuchao Li, Wei Yu, and Lefei Zhang. Bidirectional correlation-driven inter-frame inter-

- action transformer for referring video object segmentation. *Pattern Recognition*, 153:110535, 2024. 1, 2
- [21] Dezhuang Li, Ruoqi Li, Lijun Wang, Yifan Wang, Jinqing Qi, Lu Zhang, Ting Liu, Qingquan Xu, and Huchuan Lu. You only infer once: Cross-modal meta-transfer for referring video object segmentation. In *Proceedings of the AAAI Conference on Artificial Intelligence (AAAI)*, pages 1297–1305, 2022. 2
- [22] Yonglin Li, Jing Zhang, Xiao Teng, Long Lan, and Xinwang Liu. Refsam: Efficiently adapting segmenting anything model for referring video object segmentation. *arXiv preprint arXiv:2307.00997*, 2024. 2
- [23] Haotian Liu, Chunyuan Li, Qingyang Wu, and Yong Jae Lee. Visual instruction tuning. *Advances in neural information processing systems*, 36, 2024. 3
- [24] Shilong Liu, Zhaoyang Zeng, Tianhe Ren, Feng Li, Hao Zhang, Jie Yang, Qing Jiang, Chunyuan Li, Jianwei Yang, Hang Su, et al. Grounding dino: Marrying dino with grounded pre-training for open-set object detection. *arXiv preprint arXiv:2303.05499*, 2023. 2
- [25] Ilya Loshchilov and Frank Hutter. Decoupled weight decay regularization. In *ICLR*, 2018. 7
- [26] Zhuoyan Luo, Yicheng Xiao, Yong Liu, Shuyan Li, Yitong Wang, Yansong Tang, Xiu Li, and Yujiu Yang. Soc: Semantic-assisted object cluster for referring video object segmentation. *Advances in Neural Information Processing Systems*, 36, 2024. 1, 2, 3, 7
- [27] Junhua Mao, Jonathan Huang, Alexander Toshev, Oana Camburu, Alan L Yuille, and Kevin Murphy. Generation and comprehension of unambiguous object descriptions. In *Proceedings of the IEEE conference on computer vision and pattern recognition*, pages 11–20, 2016. 7
- [28] Bruce McIntosh, Kevin Duarte, Yogesh S Rawat, and Mubarak Shah. Visual-textual capsule routing for text-based video segmentation. In *Proceedings of the IEEE Conference on Computer Vision and Pattern Recognition (CVPR)*, pages 9942–9951, 2020. 2
- [29] Bo Miao, Mohammed Bennamoun, Yongsheng Gao, and Ajmal Mian. Spectrum-guided multi-granularity referring video object segmentation. In *Proceedings of the IEEE/CVF International Conference on Computer Vision*, pages 920–930, 2023. 1, 2, 7, 8
- [30] Fausto Milletari, Nassir Navab, and Seyed-Ahmad Ahmadi. V-net: Fully convolutional neural networks for volumetric medical image segmentation. In *Proceedings of the International Conference on 3D Vision (3DV)*, pages 565–571, 2016. 6
- [31] Seoung Wug Oh, Joon-Young Lee, Ning Xu, and Seon Joo Kim. Video object segmentation using space-time memory networks. In *Proceedings of the IEEE/CVF international conference on computer vision*, pages 9226–9235, 2019. 1
- [32] Jordi Pont-Tuset, Federico Perazzi, Sergi Caelles, Pablo Arbeláez, Alex Sorkine-Hornung, and Luc Van Gool. The 2017 davis challenge on video object segmentation. *arXiv preprint arXiv:1704.00675*, 2017. 6
- [33] Hanoona Rasheed, Muhammad Maaz, Sahal Shaji, Abdelrahman Shaker, Salman Khan, Hisham Cholakkal, Rao M Anwer, Eric Xing, Ming-Hsuan Yang, and Fahad S Khan. Glamm: Pixel grounding large multimodal model. In *Proceedings of the IEEE/CVF Conference on Computer Vision and Pattern Recognition*, pages 13009–13018, 2024. 3
- [34] Nikhila Ravi, Valentin Gabeur, Yuan-Ting Hu, Ronghang Hu, Chaitanya Ryali, Tengyu Ma, Haitham Khedr, Roman Rädle, Chloe Rolland, Laura Gustafson, et al. Sam 2: Segment anything in images and videos. *arXiv preprint arXiv:2408.00714*, 2024. 2, 6
- [35] Seonguk Seo, Joon-Young Lee, and Bohyung Han. Urvos: Unified referring video object segmentation network with a large-scale benchmark. In *Proceedings of the European Conference on Computer Vision (ECCV)*, pages 208–223, 2020. 2, 6, 7
- [36] Jiajin Tang, Ge Zheng, and Sibe Yang. Temporal collection and distribution for referring video object segmentation. In *Proceedings of the IEEE/CVF International Conference on Computer Vision*, pages 15466–15476, 2023. 2, 7
- [37] Di Wang, Jing Zhang, Bo Du, Minqiang Xu, Lin Liu, Dacheng Tao, and Liangpei Zhang. Samrs: Scaling-up remote sensing segmentation dataset with segment anything model. *Advances in Neural Information Processing Systems*, 36, 2024. 3
- [38] Hao Wang, Cheng Deng, Junchi Yan, and Dacheng Tao. Asymmetric cross-guided attention network for actor and action video segmentation from natural language query. In *Proceedings of the IEEE International Conference on Computer Vision (ICCV)*, pages 3939–3948, 2019. 2
- [39] Wenhui Wang, Hangbo Bao, Li Dong, Johan Björck, Zhiliang Peng, Qiang Liu, Kriti Aggarwal, Owais Khan Mohammed, Saksham Singhal, Subhojit Som, et al. Image as a foreign language: Beit pretraining for vision and vision-language tasks. In *Proceedings of the IEEE/CVF Conference on Computer Vision and Pattern Recognition*, pages 19175–19186, 2023. 4, 6
- [40] Dongming Wu, Xingping Dong, Ling Shao, and Jianbing Shen. Multi-level representation learning with semantic alignment for referring video object segmentation. In *Proceedings of the IEEE Conference on Computer Vision and Pattern Recognition (CVPR)*, pages 4996–5005, 2022. 2
- [41] Dongming Wu, Tiancai Wang, Yuang Zhang, Xiangyu Zhang, and Jianbing Shen. Onlinerefer: A simple online baseline for referring video object segmentation. In *Proceedings of the IEEE/CVF International Conference on Computer Vision*, pages 2761–2770, 2023. 7
- [42] Jiannan Wu, Yi Jiang, Peize Sun, Zehuan Yuan, and Ping Luo. Language as queries for referring video object segmentation. In *Proceedings of the IEEE Conference on Computer Vision and Pattern Recognition (CVPR)*, pages 4974–4984, 2022. 1, 2, 6, 7
- [43] Yunyang Xiong, Bala Varadarajan, Lemeng Wu, Xiaoyu Xi, Fanyi Xiao, Chenchen Zhu, Xiaoliang Dai, Dilin Wang, Fei Sun, Forrest Iandola, et al. EfficientSAM: Leveraged masked image pretraining for efficient segment anything. In *Proceedings of the IEEE/CVF Conference on Computer Vision and Pattern Recognition*, pages 16111–16121, 2024. 1, 3

- [44] Jinjin Xu, Liwu Xu, Yuzhe Yang, Xiang Li, Fanyi Wang, Yanchun Xie, Yi-Jie Huang, and Yaqian Li. u-llava: Unifying multi-modal tasks via large language model. *arXiv preprint arXiv:2311.05348*, 2023. [3](#)
- [45] Shilin Yan, Renrui Zhang, Ziyu Guo, Wenchao Chen, Wei Zhang, Hongyang Li, Yu Qiao, Hao Dong, Zhongjiang He, and Peng Gao. Referred by multi-modality: A unified temporal transformer for video object segmentation. In *Proceedings of the AAAI Conference on Artificial Intelligence*, pages 6449–6457, 2024. [7](#)
- [46] Licheng Yu, Patrick Poirson, Shan Yang, Alexander C Berg, and Tamara L Berg. Modeling context in referring expressions. In *Computer Vision–ECCV 2016: 14th European Conference, Amsterdam, The Netherlands, October 11–14, 2016, Proceedings, Part II 14*, pages 69–85. Springer, 2016. [7](#)
- [47] Seonghoon Yu, Ilchae Jung, Byeongju Han, Taeoh Kim, Yunho Kim, Dongyoon Wee, and Jeany Son. A simple baseline with single-encoder for referring image segmentation. *arXiv preprint arXiv:2408.15521*, 2024. [4](#)
- [48] Linfeng Yuan, Miaoqing Shi, Zijie Yue, and Qijun Chen. Losh: Long-short text joint prediction network for referring video object segmentation. In *Proceedings of the IEEE/CVF Conference on Computer Vision and Pattern Recognition*, pages 14001–14010, 2024. [3](#), [7](#)
- [49] Wenxi Yue, Jing Zhang, Kun Hu, Yong Xia, Jiebo Luo, and Zhiyong Wang. Surgicalsam: Efficient class promptable surgical instrument segmentation. In *Proceedings of the AAAI Conference on Artificial Intelligence*, pages 6890–6898, 2024. [3](#)
- [50] Chaoning Zhang, Dongshen Han, Yu Qiao, Jung Uk Kim, Sung-Ho Bae, Seungkyu Lee, and Choong Seon Hong. Faster segment anything: Towards lightweight sam for mobile applications. *arXiv preprint arXiv:2306.14289*, 2023. [1](#), [3](#)
- [51] Yuxuan Zhang, Tianheng Cheng, Rui Hu, Heng Liu, Longjin Ran, Xiaoxin Chen, Wenyu Liu, Xinggang Wang, et al. Evf-sam: Early vision-language fusion for text-prompted segment anything model. *arXiv preprint arXiv:2406.20076*, 2024. [2](#), [3](#), [4](#), [6](#)
- [52] Xizhou Zhu, Weijie Su, Lewei Lu, Bin Li, Xiaogang Wang, and Jifeng Dai. Deformable detr: Deformable transformers for end-to-end object detection. In *Proceedings of the International Conference on Learning Representations (ICLR)*, 2020. [2](#)